

pubs.acs.org/jcim Article

Characterizing Ion-Polymer Interactions in Aqueous Environment with Electric Fields

Valerie Vaissier Welborn,* William R. Archer, and Michael D. Schulz



Cite This: J. Chem. Inf. Model. 2023, 63, 2030-2036



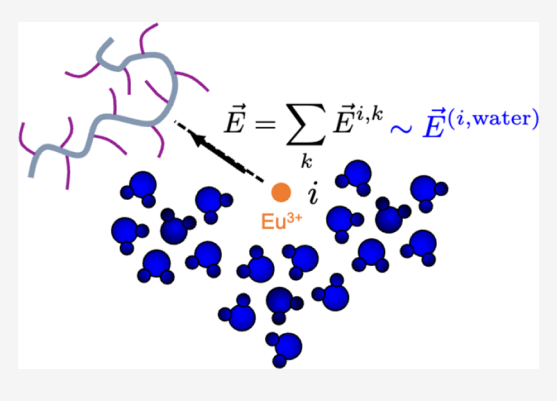
ACCESS I

Metrics & More

Article Recommendations

Supporting Information

ABSTRACT: Polymers make the basis of highly tunable materials that could be designed and optimized for metal recovery from aqueous environments. While experimental studies show that this approach has potential, it suffers from a limited knowledge of the detailed molecular interaction between polymers and target metal ions. Here, we propose to calculate intrinsic electric fields from polarizable force field molecular dynamics simulations to characterize the driving force behind Eu3+ motion in the presence of poly(ethylenimine methylenephosphonate), a specifically designed metal chelating polymer. Focusing on the metal chelation initiation step (i.e., before binding), we can rationalize the role of each molecule on ion dynamics by projecting these electric fields along the direction of ion motion. We find that the polymer functional groups act indirectly, and the polymer-metal ion interaction is actually mediated by water. This result is consistent with the



experimental observation that metal sequestration by these polymers is entropically driven. This study suggests that electric field calculations can help the design of metal chelating polymers, for example, by seeking to optimize polymer-solvent interactions rather than polymer-ion interactions.

INTRODUCTION

Synthetic metal-chelating polymers are an important technology to neutralize and remove metal contaminants from solution.¹⁻³ Several polymers have been synthesized and tested for metal sequestration applications, ⁴⁻⁶ using isothermal titration calorimetry (ITC)⁷⁻⁹ to measure the binding thermodynamics of polymers to metal ions. While ITC enables the direct measurement of heat associated with metal ion binding in solution, it is a global technique that determines the total entropy and cannot separate the competing effects of coupled events (e.g., ion binding versus (de)solvation versus polymer conformation changes). 10,11 Computational approaches can enable greater insight into polymer-metal ion interactions by focusing on time and length scales that are inaccessible to ITC or other experimental techniques. 12,13 Atomistic simulations such as molecular dynamics (MD) are well-suited to the simulation of entropic effects, ^{14–18} but the quantification of functional properties from MD is nontrivial.

$$\vec{F}(\vec{r}, t) = q\vec{E}^{\text{total}}(\vec{r}, t)$$

$$= q(\vec{E}^{\text{water}}(\vec{r}, t) + \vec{E}^{\text{polymer}}(\vec{r}, t) + ...)$$

$$= q\sum_{k} \vec{E}^{k}(\vec{r}, t)$$
(1)

In this paper, we present calculations of the electric fields experienced by metal ions in solution to identify the molecular origin of the driving force for metal capture (prior to binding), when solvated ions come into contact with solvated polymer chains (Figure 1). The decomposition of these fields into molecular contributions from the solvent, polymer chains, etc. (k), as defined in eq 1, allows us to decouple the role of water and of the polymer for a unique characterization of the early stages of metal chelation.

Despite being utilized, by us and others, to rationalize catalytic effects in proteins and supramolecular assemblies, 19-26 electric field calculations from classical MD have been seldom used in polymer modeling. This paper aims to bridge this gap, illustrating how electric field calculations in polymeric systems can yield to the identification of the driving force for metal ion motion in the presence of chelating polymers. Here, we focus on rationalizing the motion of Eu³⁺ in the presence of poly(ethylenimine methylenephosphonate) (PEI-MP), a metal-chelating polymer specifically designed to bind lanthanide ions (Figure 2). 11,27 Considering the central role of electrostatics in polymer-ion interactions in solution,²⁸⁻³³ we present electric field calculations from MD

Received: August 17, 2022

Published: December 19, 2022





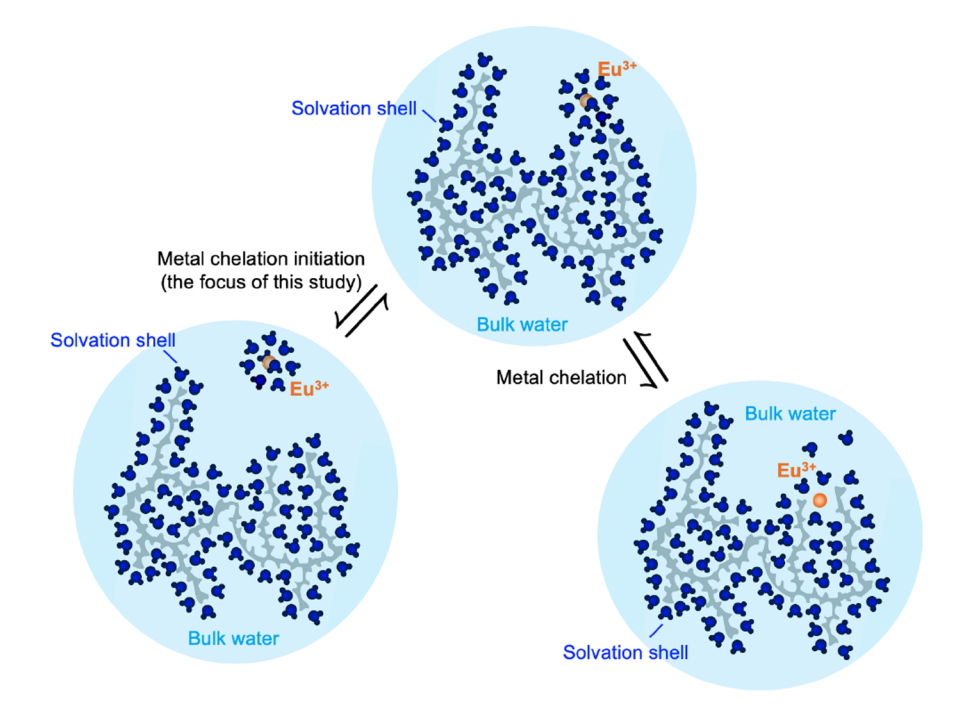


Figure 1. Metal sequestration in solution involves the rearrangement of water molecules around the metal ion and polymer chain. Here, we seek to understand the initiation of this process, where fully solvated metal ions are driven closer to the fully solvated polymer chains.

Figure 2. Chemical structure of PEI-MP.

simulations performed with the polarizable AMOEBA force field. AMOEBA incorporates atomic multipoles and induced dipoles to account for electrostatic anisotropy and electronic polarizability effects, 34–36 and parameters for solvated Eu³⁺ have already been developed and validated. 28,37

COMPUTATIONAL METHODS

AMOEBA Molecular Dynamics with Tinker. The polarizable AMOEBA force field^{34–36} as implemented in the Tinker software package³⁸ was used throughout this study. New parameters were developed when required by following the procedure detailed in ref 35 on methyl-capped PEI and PEI-MP units. These parameters are available on Zenodo, as detailed in the Data and Software Availability statement.

Five polymer chains were built starting with a 21 monomer backbone. Experiments estimate the polymer chains to be between 70 and 80% functionalized.²⁷ To mimic this property, we added a functional group on each monomer when a random number, drawn every time to be between 0 and 1, was less than 0.8. This resulted in our five polymer chains to be between 66% and 95% functionalized overall. MD simulations were run for each polymer chain for 2 ns in the NVT ensemble (Nose-Hoover thermostat, 1 fs time step, nonbonded cutoff 10 Å, beeman integrator).

Four multichain, (90 Å)³, cubic simulation cells were then built by randomly selecting one of the five polymer chains. The Debye length (λ_D) is defined as

$$\lambda_D = \sqrt{\frac{\varepsilon_r \varepsilon_0 k_B T}{\sum_j n_j^0 q_j^2}} \tag{2}$$

where ϵ_r and ϵ_0 are the relative static and vacuum permittivity, respectively, $k_{\rm B}$ is Boltzmann's constant, T is the temperature, q_j is the charge of species j, and n_j^0 is the average concentration of the charge of species j. Here, $\lambda_D=4.7$ Å, which validates our box dimension for this study (over an order of magnitude larger than the Debye length). On average, the degree of functionalization of each simulation cell reached 80% (80, 78, 80, and 74% functionalization in simulation cells 1, 2, 3 and 4, respectively), consistent with experimental systems. The starting conformation of each chain was chosen randomly from one of the 2 ns-MD trajectory conformations at 0.5, 0.75, 1.0, 1.25, or 1.5 ns. Water was added in each simulation cell water at bulk density as well as 30 Eu³⁺ and Cl⁻ ions to maintain overall charge neutrality (Figure 3). After an additional 50 ps of equilibration in the NPT ensemble, electric

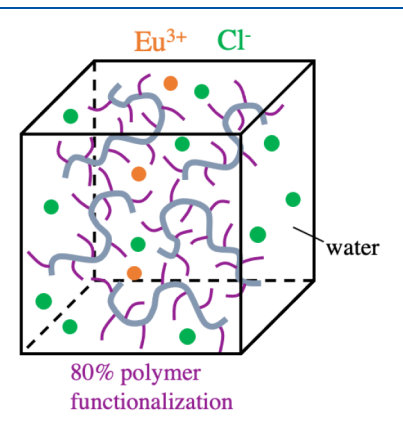


Figure 3. Schematic of the simulation cells used in this study. Each cell is $(90 \text{ Å})^3$ and contains 5 polymer chains with varying degrees of functionalization. The overall functionalization level of the cell is about 80%, as we would expect from experiments. We follow the dynamics of Eu³⁺ ions in the presence of Cl⁻ counterions.

fields were calculated over $\sim\!200$ ps (from NPT MD with Nose-Hoover thermostat, Nose-Hoover barostat, 1 fs time step, nonbonded cutoff 10 Å, beeman integrator) and compared to electric fields in a simulation cell holding 5 nonfunctionalized polymers (PEI). In the Supporting Information, we provide MD energy plots (Figure S1) as well as end-to-end polymer distance plots (Figures S2–S3) showing that our polymer chains have reached a relatively stable conformational state within these time scales. Our production MD run of 200 ps aims to analyze the dynamics of water and solvated ions in the presence of the polymer chains in these fixed conformations.

Electric Field Calculations. Electric fields were calculated every 2 ps during a 200 ps production NPT run (preceded by 50 ps equilibration) using the ELECTRIC code developed in the Welborn group.³⁹ The fields were projected onto the axis defining the minimum distance between a Eu3+ ion and a nitrogen atom from the closest polymer chain. The projection of the electric field onto this axis (a dot product operation) yields a scalar whose sign indicates the relative orientation of the field with respect to the ion-polymer direction. Negative electric field projections indicate that the electric field is oriented from the ion to the polymer, facilitating the ion coming closer to the polymer. Positive electric field projections indicate that the electric field is oriented from the polymer to the ion, facilitating the ion going away from the polymer. To gather a complete picture of ion dynamics in these systems, we calculated these projected electric fields for 2 Eu³⁺ ions that moved closer to a PEI-MP chain by over 5 Å, 2 Eu³⁺ ions that moved further away from a PEI-MP chain by over 5 Å, and 2 Eu³⁺ ions that moved less than 0.5 Å overall, in each simulation cell.

RESULTS

Polymer Conformation. In Figure 4, we show the conformation of a "bare" PEI chain with 0% functionalization (control) to the conformation of our 71 and 95% functionalized PEI-MP chains.

We observe that the presence of functional groups contracts the polymer chain, which appears more globular. However, after a functionalization threshold (\sim 85–90%), the steric hindrance and electrostatic interaction between the functional

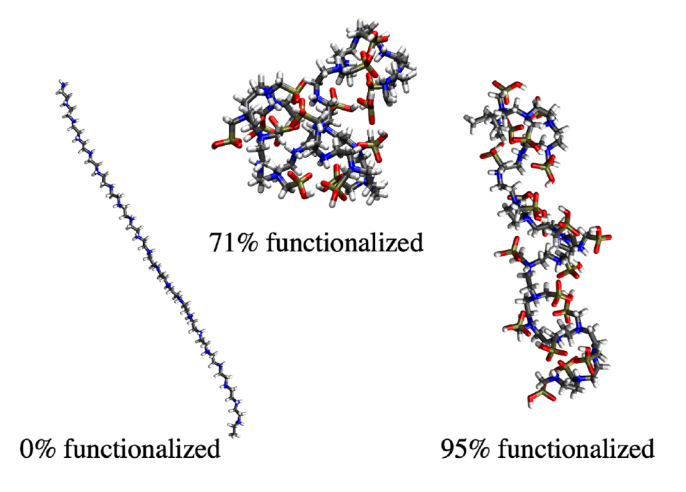
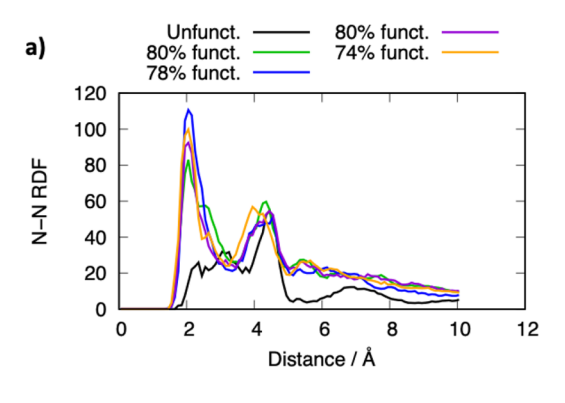


Figure 4. Polymer conformation after 1.5 ns of MD equilibration as a function of the functionalization level. Each polymer chain is 21 units long.

groups elongates the chain, similar to the linear 0% functionalized chain. As a result, the degree of functionalization dictates the overall length of the polymer chains (see Figures S2–S3) as well as the orientation of the functional groups with respect to the polymer backbone. Indeed, in more globular polymer chains, the intramolecular interactions between the nonfunctionalized repeat units and the neighboring functional groups constrain the PO₃H₂ groups to point away from the solvent, toward the backbone. In contrast, in more fully functionalized polymer chains, the PO₃H₂ groups point outward. This would suggest that more functionalized polymers are more able to interact with ions in their environment, as was observed experimentally.²⁷

Since the macroscopic properties of such systems are an ensemble average, we also characterize the polymer structure in the simulation cells that contain five polymer chains each. The N-N radial distribution function (RDF) as well as polymer—water RDF are presented in Figure 5.



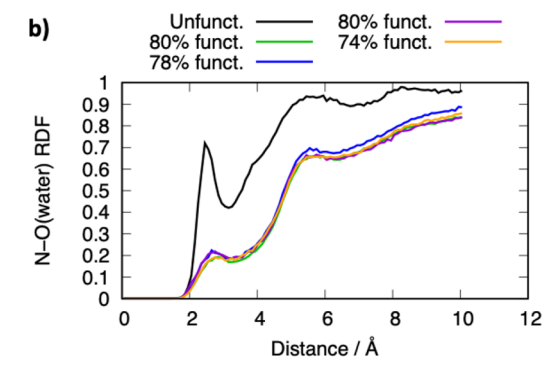


Figure 5. Radial distribution function of the 4 PEI-MP and 1 PEI simulation cells: a) polymer unit to unit RDF and b) polymer-water RDF.

We see that the four PEI-MP simulation cells have similar characteristics, with polymer chains that allow for unit-to-unit interaction as evidenced by a sharp peak at around 2 Å in the N–N RDF. The more linear PEI chains (black curve) do not share this feature. Similar observations can be made when looking at the structure of water around the chains with no significant differences between the PEI-MP cells. This validates our simulation protocol for a 80% functionalized multipolymeric solution whose properties do not depend on the specific arrangement or configuration of individual polymer chains. Meanwhile, the conformational changes due to polymer functionalization restricts water access yielding reduced structural water around the chains.

Eu³⁺ **Dynamics.** Next, we investigate the nature and magnitude of the interaction of these polymer chains with Eu³⁺ in solution. Here, we seek to characterize metal chelation initiation (Figure 1), prior to binding, as a better understanding of the origin of polymer-ion interactions would help us design systems with optimal ion capture properties. We monitor each Eu³⁺ ion during the MD by calculating the distance between Eu³⁺ and the nitrogen atom from the polymer chain closest to it, $d_{\text{ion-pol}}$. We can then quantify $d_{\text{ion-pol}}$ time evolution and count the number of metal ions that moved closer to a polymer chain, as a proxy for metal chelation initiation. The results are presented in Table 1.

Table 1. Fraction of Ions That Moved Closer to a Polymer

	Eu3+ that moved closer	$\Delta d_{ ext{ion-pol}}(ext{Å})$
PEI (control)	15%	-4.5
80% PEI-MP	52%	-6.0

"Ions that moved less than 2 Å were not counted as they are considered immobile, on average. We calculate the magnitude of the displacement, $\Delta d_{\text{ion-pol}}$ as the difference between $d_{\text{ion-pol}}$ at the end of the simulation (t_{ε}) and the beginning (t_0) : $\Delta d_{\text{ion-pol}} = d_{\text{ion-pol}}(t=t_{\varepsilon}) - d_{\text{ion-pol}}(t=t_0)$.

We observe a significant influence of the functional groups on ${\rm Eu}^{3+}$ dynamics: more than half of the ions that moved more than 2 Å in ~200 ps got closer to a PEI-MP chain, compared to only 15% when the polymers were not functionalized. Further, these ions moved, on average, 1.5 Å more in the presence of PEI-MP. This is in agreement with the ITC measurements conducted with PEI, which did not exhibit any detectable binding with ${\rm Eu}^{3+}$. 27

Looking at the local environment of a few of these Eu³⁺ ions, we cannot distinguish a specific property that could explain these findings. Indeed, all ions seem coordinated to 9 water molecules, regardless of the simulation cell and magnitude or direction of motion (see Eu-water RDF and its integration data in Figures S4–S5). What then governs the observed ion dynamics?

Molecular Origin of Eu³⁺ Dynamics. In solution, the force (\vec{F}) on a charged particle is proportional to the electric field it experiences as defined in eq 1. Here, we calculate the electric field projected along $d_{\text{ion-pol}}$ to understand the driving force behind the observed Eu^{3+} dynamics. These electric field calculations are performed as a postprocessing step on AMOEBA MD simulations using a code we recently made freely available.³⁹ Using the superposition principle, we can further split the total electric field into contributions of the system components, such as individual polymer chains, water molecules, and counterions. This allows us to rigorously identify the origin of the electrostatic interactions that bring Eu³⁺ ions closer (or further away) from PEI-MP. To reduce some of the computational cost, we compute the fields for a selection of Eu³⁺ ions, representative of the overall dynamics. We pick 2 Eu³⁺ ions that moved closer to a PEI-MP chain by over 5 Å, 2 Eu³⁺ ions that moved further away from a PEI-MP chain by over 5 Å, and 2 Eu³⁺ ions that moved less than 0.5 Å overall in each simulation cell.

First, we analyze the total electric field projections averaged over the length of the simulation and look for the main contributors, defined here as elements contributing more than 15 MV/cm in absolute value (Table 2).

Table 2. Major Contributors to the Electric Field Projected onto $d_{\text{ion-pol}}^{\ a}$

	polymer chain	water	other ions
PEI (control)	18.4%	79.8%	1.8%
80% PEI-MP	17.8%	79%	3.2%

"We searched for any molecule, ion, or polymer chain contributing more than 15 MV/cm (in absolute value) to the total field. The percentage presented here is the proportion of each type of molecule for these high contributors.

On average, the water contributes up to 4 times as much as the polymer chain to Eu³⁺ dynamics, regardless of the degree of functionalization of the polymers and the direction of motion. Further splitting the water data from Table 2 into contributions from individual molecules (see the Supporting Information for details about electric field data analysis with decomposition into molecular contributions), we note that a limited number of water molecules make this number, between 2 and 6, depending on the case. In Figure 6, we show the position of these water molecules with respect to Eu³⁺, and we observe that these waters mostly belong to the first solvation shell of the Eu³⁺ ion.

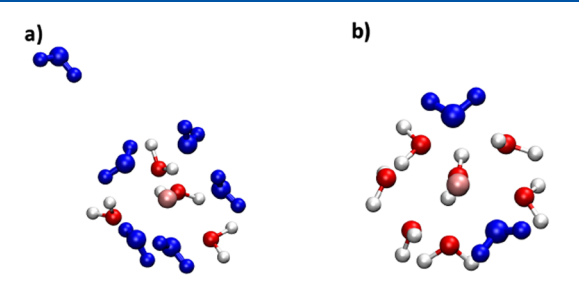


Figure 6. Visualization of the highest contributors (blue) to the projected electric field. A few water molecules make the most of this contribution, mostly from the first coordination shell of the ion: 5 out of 6 in case a) and 2 out of 2 in case b).

Second, we analyze the time evolution of the projected electric field to identify the spontaneous changes that lead to ion motion. Focusing on the relative contribution of the polymer chains within one simulation cell, we show the time evolution of the total electric field (brown) and the electric field emanating from each polymer chains in Figure 7.

We see that only one polymer chain contributes to the total electric field in each case, suggesting that we are modeling single chain effects on ion sequestration. Experimentally, polymer aggregation has been observed when adding metal ions in the system.²⁷ In this case, we would expect an even more complex picture with potential collaborative effects between polymer chains upon ion binding. However, the present model aims to portray the initiation of metal chelation, prior to binding or aggregation, and we restrict ourselves to the role of a single chain on Eu³⁺ dynamics.

Note that the total electric fields fluctuate widely on the picosecond time scale as the simulation evolves. This is because the magnitude and orientation of the fields are very sensitive to the system geometry, which partly explains why they are such a good metric to link structure to function in condensed phase systems. Here, we look beyond these picosecond fluctuations, for larger variations over tens of picoseconds that characterize ion motion in the system. In Figure 8, we show the time evolution of each field component

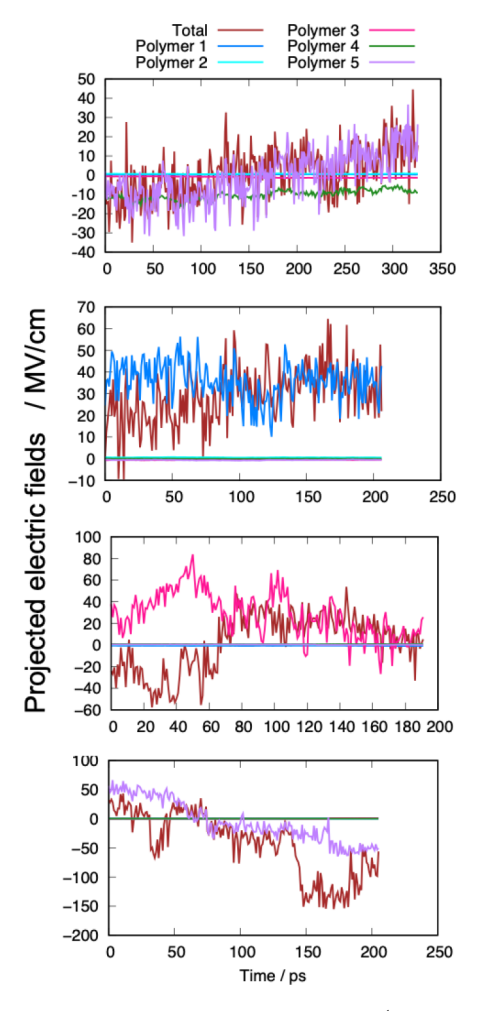


Figure 7. Time evolution of the total electric field (all polymer chains, water, and ions) and polymer contribution to the electric field, projected along the Eu³⁺-polymer direction. Negative projections mean that the electric field supports the ion moving closer to the polymer, while positive projections mean that the electric field supports the ion moving away from the polymer. From top to bottom: PEI-MP simulation cell 1, PEI-MP simulation cell 2, PEI-MP simulation cell 3, and PEI-MP simulation cell 4.

overlapped with the time evolution of $d_{\text{ion-pol}}$ (additional plots are provided in the Supporting Information, Figures S7–S11).

Overall, the dominant contributions to negative electric field projections (i.e., contribution to projections that facilitate Eu³⁺ motion toward the polymer) come from water and Cl⁻ ions, in that order. This contrasts with the contribution from the polymer chains that is often positive. Note that this is a global observation that is not true always: in some cases, like the last 150 ps in Figure 8a, Figure S7 (first case) and Figure S10 (second case), the polymer field projection is negative, while the water field projection is positive. However, more often than not, we see that the water field helps drive the ions closer, while the polymer field pushes them away.

In addition to the overall sign of the electric field projections, we can analyze the variations in field contributions with respect to variations in $d_{\text{ion-pol}}$ within each plot. In Figure 8a (first 200 ps), Figure 8b, Figure 8d (first 200 ps), and Figure 8e (last 140 ps), variations in $d_{\text{ion-pol}}$ follow closely the fluctuations of the water field. Meanwhile, the Cl⁻ counterion field seems to drive the evolution of $d_{\text{ion-pol}}$ during the first 40 ps in Figure 8c, and the polymer field drives the evolution of

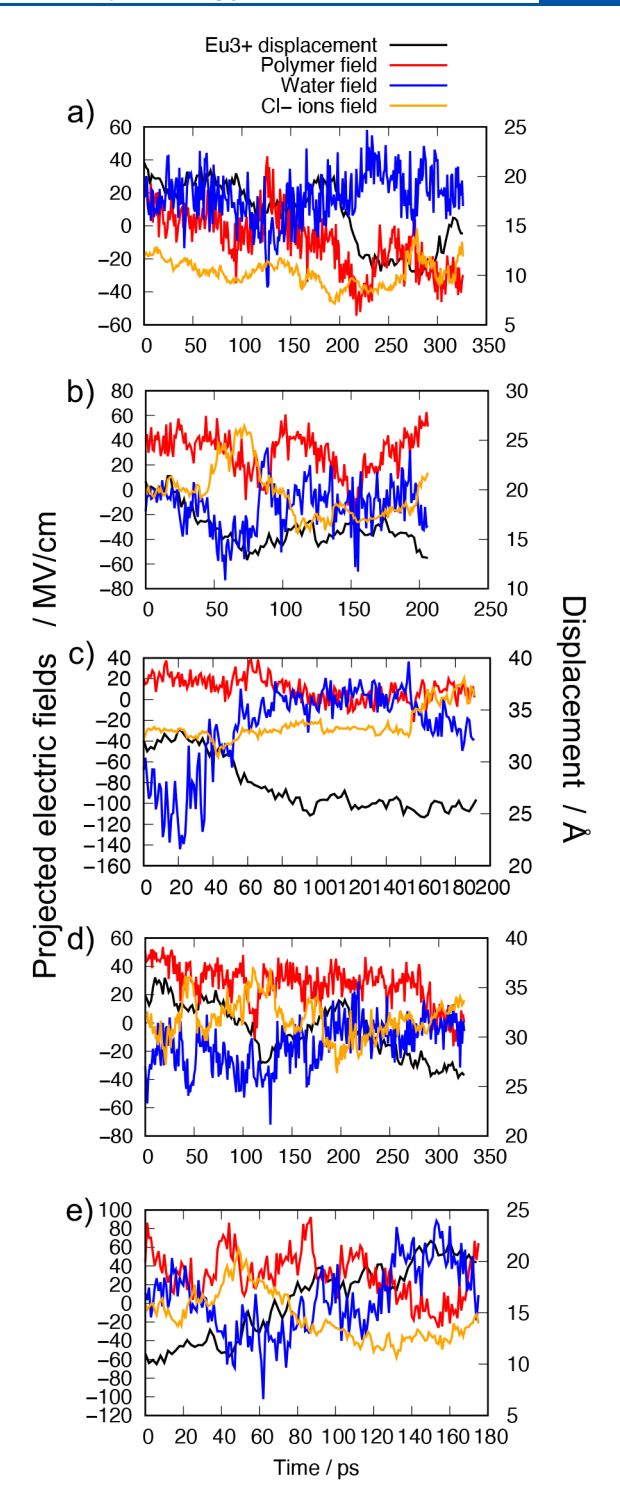


Figure 8. Time evolution of the electric field components projected along the $\mathrm{Eu^{3+}}$ -polymer direction (axis on the left) and time evolution of $d_{\mathrm{ion\text{-}pol}}$ (axis on the right). Negative projections mean that the electric field supports the ion moving closer to the polymer, while positive projections mean that the electric field supports the ion moving away from the polymer. (a)-(d) PEI-MP simulation cells 1–4 and (e) PEI simulation cell.

 $d_{\rm ion\text{-}pol}$ at the 200 ps mark in Figure 8a and after 60 ps in Figure 8c. We also note that the field emanating from the counterions in Figure 8b, Figure 8d, and Figure 8e varies substantially, but neither variation is followed by a variation in $d_{\rm ion\text{-}pol}$. Similar observations can be made from the additional plots provided in

the Supporting Information (Figures S7-S11). Although the polymer field can yield negative projections, and the polymer and Cl⁻ fields can drive variations in $d_{\text{ion-pol}}$, the water field is responsible for Eu³⁺-dynamics for the majority of the time. Combining these observations with our previous findings where we saw a significant influence of the presence of functional groups in attracting Eu³⁺ ions (Table 1), we believe that the functional groups help in directing the electric field emanating from the water molecules. In other words, the presence of the functionalized polymers helps to bias the orientation of the water fields toward the polymer (Figure S11 shows an almost equal amount of positive and negative water field projections in the PEI cell), which would otherwise be randomly oriented around the ions (isotropic distribution of water molecules in solution). This means that the ions feel a cooperative effect of the polymer and water that affects the early stage of metal chelation. This interpretation is consistent with the experimental observation that Eu³⁺ binding, as measured by ITC, is entropic.

CONCLUSION

In summary, we presented a series of electric field calculations that help identify the molecular driving force at the origin of metal chelation in solution. This is because polymeric systems consist of polar and polarizable fragments that are described in polar (aqueous) environments by permanent and induced dipoles. The relative orientation and magnitude of these dipoles adapt to changes in geometry as the system evolves in time, modulating the resulting electric field. It follows that information about the electric field exerted on an ion can be used to predict ion dynamics.

Here, we used this principle and calculated electric field projections to understand Eu³⁺ dynamics in the presence of PEI-MP chains. We saw that while polymer chains can occasionally govern Eu³⁺ motion, it is the water molecules that are primarily responsible for Eu³⁺ dynamics. This means that the significant influence of the polymer functional groups on Eu3+ dynamics is an indirect effect. Indeed, our simulations suggest that highly functionalized polymers adopt conformations that better expose their functional groups to solvent. This exposure creates strong polymer-water interactions and disrupts the network of water molecules, which is at the origin of Eu³⁺ motion. This would suggest that the entropic origin of ion binding observed experimentally comes from water rearrangement around the polymer chains. Further work involves looking at the water structure and hydrogen bonding networks upon binding in simpler cases to further isolate the key contributions to metal chelation.

■ DATA AND SOFTWARE AVAILABILITY

The ELECTRIC code used to compute the electric field from Tinker AMOEBA trajectories is available free of charge on Github [https://github.com/WelbornGroup/ELECTRIC.git]. MD input and parameter files from Tinker 8 are available on Zenodo [10.5281/zenodo.7278373].

ASSOCIATED CONTENT

Supporting Information

The Supporting Information is available free of charge at https://pubs.acs.org/doi/10.1021/acs.jcim.2c01048.

Total energy and end-to-end polymer MD plots, radial distribution functions (PDF)

AUTHOR INFORMATION

Corresponding Author

Valerie Vaissier Welborn – Department of Chemistry, Macromolecules Innovation Institute (MII), Virginia Tech, Blacksburg, Virginia 24060, United States; orcid.org/ 0000-0003-0834-4441; Email: vwelborn@vt.edu

Authors

William R. Archer — Department of Chemistry, Macromolecules Innovation Institute (MII), Virginia Tech, Blacksburg, Virginia 24060, United States; orcid.org/ 0000-0002-6326-6602

Michael D. Schulz – Department of Chemistry, Macromolecules Innovation Institute (MII), Virginia Tech, Blacksburg, Virginia 24060, United States; orcid.org/ 0000-0001-8499-6025

Complete contact information is available at: https://pubs.acs.org/10.1021/acs.jcim.2c01048

Notes

The authors declare no competing financial interest.

ACKNOWLEDGMENTS

The authors thank the Virginia Tech Department Faculty Start-up Funds, GlycoMIP, a National Science Foundation Materials Innovation Platform funded through Cooperative Agreement DMR-1933525, and the U.S. Department of Energy, Office of Science, Office of Basic Energy Sciences, under Award Number DE-SC0023035, for financial support. The authors also acknowledge Advanced Research Computing at Virginia Tech for providing computational resources and technical support that have contributed to the results reported within this paper. Finally, the authors thank Prof. Richard Gandour for helpful discussions during the preparation of this manuscript.

REFERENCES

- (1) Barakat, M. A. New trends in removing heavy metals from industrial wastewater. *Arab. J. Chem.* **2011**, *4*, 361–377.
- (2) Fu, F.; Wang, Q. Removal of heavy metal ions from wastewaters: A review. J. Environ. Manage. 2011, 92, 407–418.
- (3) Byrne, F. P.; Assemat, Jamie MZ; Stanford, Amy E; Farmer, Thomas J; Comerford, James W; Pellis, Alessandro Enzyme-catalyzed synthesis of malonate polyesters and their use as metal chelating materials. *Green Chem.* **2021**, *23*, 5043–5048.
- (4) Archer, W. R.; Hall, Brady A.; Thompson, Tiffany N.; Wadsworth, Ophelia J.; Schulz, Michael D. Polymer sequestrants for biological and environmental applications. *Polym. Int.* **2019**, *68*, 1220–1237.
- (5) Hasan, I.; Ahamd, Rais A facile synthesis of poly (methyl methacrylate) grafted alginate@ Cysbentonite copolymer hybrid nanocomposite for sequestration of heavy metals. *Groundwater for Sustainable Development* **2019**, *8*, 82–92.
- (6) Nchoe, O. B; Klink, Michael J; Mtunzi, Fanyana M; Pakade, Vusumzi E Synthesis, characterization, and application of β -cyclodextrin-based ion-imprinted polymer for selective sequestration of Cr (VI) ions from aqueous media: Kinetics and isotherm studies. *J. Mol. Liq.* **2020**, 298, 111991.
- (7) Chiad, K.; Stelzig, Simon H; Gropeanu, Radu; Weil, Tanja; Klapper, Markus; Mullen, Klaus Isothermal titration calorimetry: a powerful technique to quantify interactions in polymer hybrid systems. *Macromolecules* **2009**, *42*, 7545–7552.
- (8) Arnaud, A.; Bouteiller, Laurent Isothermal titration calorimetry of supramolecular polymers. *Langmuir* **2004**, *20*, *6858*–*6863*.

- (9) Velázquez-Campoy, A.; Ohtaka, Hiroyasu; Nezami, Azin; Muzammil, Salman; Freire, Ernesto Isothermal titration calorimetry. *Current protocols in cell biology* **2004**, 23, 17–8.
- (10) Archer, W. R.; Schulz, Michael D. Isothermal titration calorimetry: practical approaches and current applications in soft matter. *Soft Matter* **2020**, *16*, 8760–8774.
- (11) Archer, W. R.; Gallagher, Connor MB.; Welborn, V Vaissier.; Schulz, Michael D. Exploring the role of polymer hydrophobicity in polymer—metal binding thermodynamics. *Phys. Chem. Chem. Phys.* **2022**, *24*, 3579.
- (12) Ketkar, P. M; Shen, Kuan-Hsuan; Fan, Mengdi; Hall, Lisa M; Epps, Thomas H, III Quantifying the Effects of Monomer Segment Distributions on Ion Transport in Tapered Block Polymer Electrolytes. *Macromolecules* **2021**, *54*, 7590–7602.
- (13) Pluharova, E.; Jungwirth, Pavel; Matubayasi, Nobuyuki; Marsalek, Ondrej Structure and dynamics of the hydration shell: Spatially decomposed time correlation approach. *J. Chem. Theory Comput.* **2019**, *15*, 803–812.
- (14) Braun, E.; Gilmer, Justin.; Mayes, Heather B.; Mobley, David L.; Monroe, Jacob I.; Prasad, Samarjeet.; Zuckerman, Daniel M. Best practices for foundations in molecular simulations [Article v1. 0]. *LiveCoMS* **2019**, *1*, 5957.
- (15) Schäfer, H.; Mark, Alan E; Gunsteren, Wilfred F van Absolute entropies from molecular dynamics simulation trajectories. *J. Chem. Phys.* **2000**, *113*, 7809–7817.
- (16) Levy, R. M; Karplus, Martin; Joseph, Kushick; Perahia, David Evaluation of the configurational entropy for proteins: application to molecular dynamics simulations of an α -helix. *Macromolecules* **1984**, 17, 1370–1374.
- (17) Kantardjiev, A.; Ivanov, Petko M Entropy rules: Molecular dynamics simulations of model oligomers for thermoresponsive polymers. *Entropy* **2020**, 22, 1187.
- (18) Kirby, B. J; Jungwirth, Pavel Charge scaling manifesto: A way of reconciling the inherently macroscopic and microscopic natures of molecular simulations. *J. Phys. Chem. Lett.* **2019**, *10*, 7531–7536.
- (19) Lawal, M. M.; Welborn, Valerie Vaissier Structural Dynamics Support Electrostatic Interactions in the Active Site of Adenylate Kinase. *ChemBioChem.* **2022**, *23*, e202200097.
- (20) Vaissier Welborn, V. Structural dynamics and computational design of synthetic enzymes. *Chem. Catalysis* **2022**, *2*, 19–28.
- (21) Welborn, V. V.; Ruiz Pestana, Luis; Head-Gordon, Teresa Computational optimization of electric fields for better catalysis design. *Nat. Catal.* **2018**, *1*, 649–655.
- (22) Vaissier, V.; Sharma, Sudhir C; Schaettle, Karl; Zhang, Taoran; Head-Gordon, Teresa Computational optimization of electric fields for improving catalysis of a designed kemp eliminase. *ACS Catal.* **2018**, *8*, 219–227.
- (23) Welborn, V. V.; Li, Wan-Lu; Head- Gordon, Teresa Interplay of water and a supramolecular capsule for catalysis of reductive elimination reaction from gold. *Nat. Commun.* **2020**, *11*, 415.
- (24) Fried, S. D.; Bagchi, Sayan; Boxer, Steven G Extreme electric fields power catalysis in the active site of ketosteroid isomerase. *Science* **2014**, *346*, 1510–1514.
- (25) Wu, Y.; Fried, Stephen D; Boxer, Steven G A preorganized electric field leads to minimal geometrical reorientation in the catalytic reaction of ketosteroid isomerase. *J. Am. Chem. Soc.* **2020**, 142, 9993–9998.
- (26) Hennefarth, M. R.; Alexandrova, Anastassia N Direct Look at the Electric Field in Ketosteroid Isomerase and Its Variants. *ACS Catal.* **2020**, *10*, 9915–9924.
- (27) Archer, W. R.; Fiorito, Agustin; Sherrie, L.; Heinz-Kunert; MacNicol, Piper L.; Winn, Samantha A.; Schulz, Michael D. Synthesis and Rare-Earth-Element Chelation Properties of Linear Poly-(ethylenimine methylenephosphonate). *Macromolecules* **2020**, *53*, 2061–2068.
- (28) Marjolin, A.; Gourlaouen, Christophe; Clavaguéra, Carine; Ren, Pengyu Y; Piquemal, Jean-Philip; Jean-Pierre, Dognon Hydration gibbs free energies of open and closed shell trivalent

- lanthanide and actinide cations from polarizable molecular dynamics. *J. Mol. Model.* **2014**, *20*, 1–7.
- (29) Qiao, B.; Skanthakumar, S.; Soderholm, L. Comparative CHARMM and AMOEBA simulations of lanthanide hydration energetics and experimental aqueoussolution structures. *J. Chem. Theory Comput.* **2018**, *14*, 1781–1790.
- (30) Melcr, J.; Martinez-Seara, Hector; Nencini, Ricky; Kolafa, Jiří; Jungwirth, Pavel; Samuli Ollila, O. H. Accurate binding of sodium and calcium to a POPC bilayer by effective inclusion of electronic polarization. *J. Phys. Chem. B* **2018**, *122*, 4546–4557.
- (31) Melcr, J.; Ferreira, Tiago M; Jungwirth, Pavel; Samuli Ollila, O. H. Improved cation binding to lipid bilayers with negatively charged POPS by effective inclusion of electronic polarization. *J. Chem. Theory Comput.* **2020**, *16*, 738–748.
- (32) Gebala, M.; Herschlag, Daniel Quantitative studies of an RNA duplex electrostatics by ion counting. *Biophys. J.* **2019**, *117*, 1116–1124.
- (33) Ma, C. Y.; Pezzotti, Simone; Schwaab, Gerhard; Gebala, Magdalena; Herschlag, Daniel; Havenith, Martina Cation enrichment in the ion atmosphere is promoted by local hydration of DNA. *Phys. Chem. Chem. Phys.* **2021**, *23*, 23203–23213.
- (34) Ponder, J. W.; Wu, Chuanjie; Ren, Pengyu; Pande, Vijay S; Chodera, John D; Schnieders, Michael J; Haque, Imran; Mobley, David L; Lambrecht, Daniel S; DiStasio, Robert A, Jr; Head-Gordon, Martin; Gary, N.; Clark, I.; Johnson, Margaret E.; Head-Gordon, Teresa Current status of the AMOEBA polarizable force field. *J. Phys. Chem. B* **2010**, *114*, 2549–2564.
- (35) Zhang, C.; Lu, Chao; Jing, Zhifeng; Wu, Chuanjie; Piquemal, Jean-Philip; Ponder, Jay W; Ren, Pengyu AMOEBA polarizable atomic multipole force field for nucleic acids. *J. Chem. Theory Comput.* **2018**, *14*, 2084–2108.
- (36) Laury, M. L.; Wang, Lee-Ping; Pande, Vijay S; Head-Gordon, Teresa; Ponder, Jay W Revised parameters for the AMOEBA polarizable atomic multipole water model. *J. Phys. Chem. B* **2015**, 119, 9423–9437.
- (37) Marjolin, A.; Gourlaouen, Christophe; Clavaguéra, Carine; Ren, Pengyu Y; Wu, Johnny C; Gresh, Nohad; Jean-Pierre, Dognon; Piquemal, Jean-Philip Toward accurate solvation dynamics of lanthanides and actinides in water using polarizable force fields: from gas-phase energetics to hydration free energies. *Theor. Chem. Acc.* 2012, 131, 1198.
- (38) Rackers, J. A.; Wang, Zhi; Lu, Chao; Laury, Marie L; Lagardere, Louis; Schnieders, Michael J; Piquemal, Jean-Philip; Ren, Pengyu; Ponder, Jay W Tinker 8: software tools for molecular design. *J. Chem. Theory Comput.* **2018**, *14*, 5273–5289.
- (39) Nash, J.; Taylor, Barnes; Welborn, Valerie Vaissier ELECTRIC: Electric fields Leveraged from multipole Expansion Calculations in Tinker Rapid Interface Code. *J. Open Source Softw.* **2020**, *5*, 2576.